Songklanakarin J. Sci. Technol.
44 (5), 1225–1231, Sep. – Oct. 2022

http://www.sjst.psu.ac.th

Original Article

Biopolymer-based corrosion inhibitor from chitosan grafted with poly(2-hydroxyethylmethacrylate) (CS-*g*-PHEMA) synthesized by ultrasound-assisted method

Sani Nazifi Dalhatu[1], Santi Khoonsap[2, 3], Siriwimol Suwannarat[2, 3], Sujitra Amnuaypanich[2], and Sittipong Amnuaypanich[2, 3*]

[1] *Department of Chemistry, Faculty of Science, Kano University of Science and Technology Wudil, Kano State, 713281 Nigeria*

[2] *Department of Chemistry and Center of Excellence for Innovation in Chemistry (PERCH-CIC), Faculty of Science, Khon Kaen University, Mueang, Khon Kaen, 40002 Thailand*

[3] *Materials Chemistry Research Center (MCRC-KKU), Faculty of Science, Khon Kaen University, Mueang, Khon Kaen, 40002 Thailand*

Received: 18 May 2022; Revised: 13 July 2022; Accepted: 5 August 2022

Abstract

A biopolymer-based corrosion inhibitor was developed from CS grafted with PHEMA. The CS-*g*-PHEMA was successfully synthesized by using an ultrasound-assisted method. The synthesized CS-*g*-PHEMA was employed as corrosion inhibitor for mild steel. The corrosion test by gravimetry under 0.2 M H_2SO_4 revealed that, in comparison with CS, the inhibition efficiency of CS-*g*-PHEMA was higher reaching 90% at 500 ppm, while the corrosion rate with CS-*g*-PHEMA was reduced to a half. Furthermore, E_a of the corrosion was higher with CS-*g*-PHEMA compared to that with CS, indicating a higher energy barrier for the corrosion reactions. The potentiodynamic polarization measurement clearly showed a superior effect of CS-*g*-PHEMA on retarding anodic oxidation and cathodic reduction on the mild steel surface. This is because adsorbed CS-*g*-PHEMA limits the diffusion of H_3O^+ to participate in anodic metal dissolution or cathodic hydrogen evolution on the mild steel surface.

Keywords: ultrasound, chitosan, poly(2-hydroxyethylmethacrylate), corrosion inhibitors, biopolymers

1. Introduction

Mild steel is carbon steel with a low amount of carbon, typically in the range of 0.05 – 0.25 wt.%. A widely-used construction material, mild steel possesses ductility and weldability with a relatively low cost compared with other types of steels. The susceptibility to oxidation of mild steel, however, deters its use, particularly when exposed to an acidic environments, for instance during acid cleaning, acid pickling, or oil well acidification. Not only are strength and lifetime of mild steel adversely affected by corrosion, but additional expenses are incurred from controlling or preventing corrosion. Several methods have been employed to mitigate the corrosion of steel. Among the methods to counteract corrosion, corrosion inhibitors have proven to be effective and yet low-cost (Kausalya & Hazlina, 2020). Corrosion inhibitors are compounds applied on the metal surface at a low concentration, capable of preventing metal dissolution and oxidation. When adsorbed on the steel surface, the corrosion inhibitor behaves as a protective barrier that impedes the initiation of corrosion reactions (Devi, Sharma, & Singh, 2016). Synthetic organic compounds have been utilized as

*Corresponding author
Email address: asitti@kku.ac.th

corrosion inhibitors since they contain nucleophilic functional groups or conjugated double or triple bonds, which supply electrons to inhibit the corrosion redox reactions (Yadav, Sharma, & Yadav, 2013). However, toxicity and high price of most synthetic corrosion inhibitors may discourage their use, while it encourages the search for alternate materials that would be non-toxic, sustainable, and low-cost.

Biopolymers are good candidates for corrosion inhibitors, and so is in particular chitosan (CS) due to its non-toxicity, and being a sustainable resource and low cost (Umoren, Banera, & Gervasi, 2013). CS is a linear polysaccharide containing specific functional groups with lone pair electrons, i.e., -NH_2 and -OH, which can form strong bonds to the metal surface (Rabizadeh & Khameneh Asl, 2019). To improve metal surface adhesion and reduce metal dissolution, CS has been modified by various methods, for example to composites with metal ions or metal oxides (Chang, Niu, Huang, & Kuo, 2007), by functionalization (Alguaci, 2020), and by blending or graft copolymerization with other polymers (Abdallah, Fawzy, & Hawsawi, 2020). Among these methods, grafting offer a variety of functional groups under facile reaction conditions.

The grafting of a polymer on CS is readily performed by the grafting-from method via typical thermal or redox initiation (Argüelles-Monal, Lizardi-Mendoza, Fernández-Quiroz, Recillas-Mota, & Montiel-Herrera, 2018). Alternatively, the polymer grafting can be achieved by an ultrasound-assisted method. Ultrasound (US) has a frequency beyond the range of human hearing generally is in the range from 20 kHz to 500 MHz. Irradiation by ultrasound induces the formation of miniscule gas bubbles in a liquid medium, which grow to a critical size and then collapse or implode; this is known as acoustic cavitation. The collapsing bubble is so intense as to produce extreme but transient conditions of very high local temperatures (5000 °C) and pressures (1000 atm) so-called hot spots (Xu, Zhang, Guo, Feng, & Tan, 2019). The hot spots enable various chemical effects in seemingly ambient conditions, offering a vast spectrum of alternative material synthesis reactions (Mason & Lorimer, 2002), including ultrasound-assisted polymerization. The intense conditions in a hot spot can decompose initiators into active radicals, a process known as sonolysis. In the presence of vinyl monomers, thus, these active radicals can initiate the graft polymerization on existing polymer chains (McKenzie, Karimi, Ashokkumar, & Qiao, 2019).

In the present study, the ultrasound-assisted method was utilized, for the first time, to graft a hydrophilic polymer on chitosan. The ultrasound-assisted grafting of poly(2-hydroxyethylmethacrylate) on CS was explored and it proved to be more effective than the conventional thermal-initiation method. CS-*g*-PHEMA was further employed as a biopolymer-based corrosion inhibitor on mild steel. The corrosion testing was performed by both gravimetry as well as electrochemical methods. Owing to the abundant hydroxyl groups on the grafted PHEMA, CS-*g*-PHEMA was preferentially adsorbed on the mild steel surface and thus provided superior corrosion inhibition to that by CS. CS-*g*-PHEMA was able to retard anodic oxidation and cathodic reduction on the mild steel surface by limiting the diffusion of H^+ ions to undergo anodic metal dissolution and cathodic hydrogen evolution.

2. Materials and Methods

2.1 Materials

Chitosan with medium molecular weight and 2-hydroxyethylmethacrylate monomer (HEMA, 97%) were purchased from Sigma Aldrich. The HEMA monomer was purified by passing through an alumina column under nitrogen flushing. Tert-Butyl hydroperoxide (TBHP, 70 wt.% aqueous solution) was purchased from Acros Organics. Sodium hydroxide, acetic acid and sulfuric acid were supplied by Ajex Finechem and by Sigma Aldrich.

2.2 Ultrasound-assisted grafting of PHEMA on CS (Cs-g-PHEMA)

The grafting of PHEMA onto CS was carried out under indirect ultrasound irradiation. The ultrasound vessel consisted of a stainless-steel planar transducer (Acme-Korn, Thailand) submerged in a temperature-controlled water bath. The transducer provided ultrasonic wave at 20 kHz frequency with a dissipation power of 27.0 W (intensity = 0.2 W/cm^2) determined by calorimetry (Kimura *et al*., 1996). 1.0 g of CS was dissolved completely in 100 ml of 0.1 M acetic acid solution in an Erlenmeyer flask, prior to adding 1 ml of TBHP solution. The flask was placed on the planar transducer and subjected to US for 20 min. Next, a designated amount of HEMA was added into the flask, and then the US irradiation was continued for a designated time period to perform the grafting. As-synthesized graft copolymer was precipitated out of the solution using 0.5 M NaOH and was collected on a filter paper. The graft polymer was then dried in an oven at 60 °C for 24 h. Ungrafted PHEMA (homo-PHEMA) was removed by Soxhlet extraction with deionized water at 90 °C for 12 h. After the extraction, CS-*g*-PHEMA was obtained and was then dried in oven at 60 °C for 6 h followed by drying in vacuum oven at 60 °C overnight. The grafting percentage (GP) and the grafting efficiency (GE) of PHEMA on CS were calculated according to the equations:

$$\text{GP (\%)} = \frac{W_{gcs} - W_{cs}}{W_{cs}} \times 100 \quad (1)$$

$$\text{GE (\%)} = \frac{W_{gcs} - W_{cs}}{W_{HEM}} \times 100 \quad (2)$$

where W_{CS}, W_{gCS} and W_{HEMA} are the weights of CS, CS-*g*-PHEMA and HEMA monomer, respectively.

2.3 Characterization

Chemical structure of CS-*g*-PHEMA was analyzed by using attenuated total reflection Fourier transform infrared spectroscopy (ATR-FTIR), with a Bruker FTIR spectrometer (Tensor 27). Thermal analysis was performed on a TG/DTA thermogravimetric analyzer, Hitashi (STA7200), under nitrogen atmosphere using a heating rate of 10 ºC/min and temperature range from 25 °C to 600 °C.

2.4 Corrosion test

2.4.1 Gravimetry method

Mild steel coupons of size 3.0 x 2.0 cm and 0.4 cm thick were mechanically polished with different grades of SiC (200–600) emery papers, and then successively washed with acetone and deionized water before drying in oven at 60 °C for 1 h. CS-*g*-PHEMA was dissolved in 100 ml of 0.2 M H_2SO_4 solution. Then, the mild steel coupons were immersed into the solution and were incubated in the solution at 25 °C for a designated period of time. After that the coupons were removed from the solutions, washed with deionized water prior to drying in an oven at 60 °C for 1 h, and weighed again. The same procedure was also performed with CS and without inhibitors (blank). The gravimetry test was repeated in triplicate. The weight loss (ΔW) was determined as the weight difference between the weights of the coupon before (dried coupon) and after the incubation. Accordingly, the corrosion rate (R_{cor}) and the inhibition efficiency (IE) were calculated using equations (3) and (4), respectively.

$$R_{cor} = \frac{\Delta W}{A \times t} \quad (3)$$

$$IE\ (\%) = \frac{R_{cor2} - R_{cor1}}{R_{cor1}} \times 100 \quad (4)$$

where A is the exposed area of the mild steel coupon (cm^2), t is incubation time (h), and R_{cor1} and R_{cor2} are the corrosion rates without and with inhibitors, respectively. The surface coverage (θ) was determined from the ΔW divided by the weight of dried coupon.

2.4.2 Potentiodynamic polarization measurement

Potentiodynamic polarization runs were conducted on Autolab PGSTAT302N potentiostat (Metrohm, The Netherland) using NOVA 1.9 software. The apparatus has three electrodes including Ag/AgCl (3 M KCl) as a reference electrode, the mild steel coupon with 1.0 cm^2 exposed area as the working electrode, and a copper wire as the counter electrode. The open-circuit potential was monitored until reaching steady state. The measurements were performed within the potential range from -0.5 V to +0.5 V using a scan rate of 0.01 Vs^{-1} at room temperature. Tafel plots were constructed and the anodic Tafel slope (β_a), cathodic Tafel slope (β_c) and corrosion current density (i_{corr}) were evaluated from the intercept of extrapolated cathodic and anodic lines at the corrosion potential (E_{cor}). The potentiodynamic corrosion inhibition efficiency (IE_P) was accordingly determined by equation (5).

$$IE_P\ (\%) = \frac{i^0_{cor} - i_{cor}}{i^0_{cor}} \times 100 \quad (5)$$

where i^0_{cor} and i_{cor} are the corrosion current densities of the mild steel in the absence and presence of the inhibitor, respectively.

3. Results and Discussion

3.1 Ultrasound-assisted grafting of PHEMA on CS

The mechanism of PHEMA grafting on CS is illustrated schematically in Figure 1. Unlike the thermal decomposition of TBHP, which requires a temperature as high as 80 °C, TBHP in the presence of ultrasound dissociates into hydroxyl and t-butoxy radicals under ambient temperature due to the chemical effects of acoustic cavitation. The radicals then abstract protons from either secondary hydroxyl of C3 or primary hydroxyl of C6 or amino group of C2 on the CS backbone, which generates active grafting sites (Li, Elango, & Wu, 2020). Graft polymerization is then initiated as HEMA monomers in solution approach the active grafting sites on CS backbones. The PHEMA chains are growing from the grafting sites on CS backbones during propagation of the radical polymerization. The growth of grafted-PHEMA chains is terminated by a combination or disproportionation with other active grafted-chains or active oligomers (Sanaeishoar, Sabbaghan, & Argyropoulos, 2018).

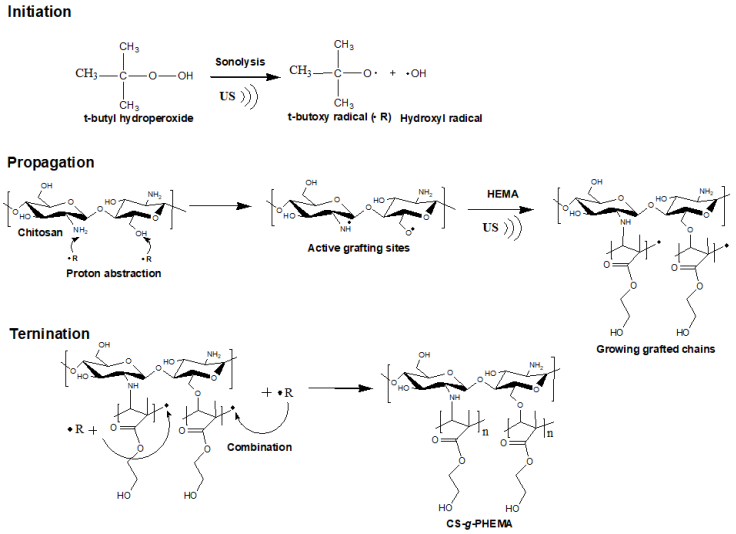

Figure 1. Schematic representation of ultrasound-assisted grafting of PHEMA onto CS

3.1.1 Characterization

The FT-IR spectrum of CS-*g*-PHEMA is shown in Figure 2 along with those of CS and PHEMA. The characteristic IR peaks of CS were observed at 1656 cm^{-1} and 1591 cm^{-1} belonging respectively to C=O stretching and -NH bending, while the broad peak at 3356 cm^{-1} corresponds to -OH and -NH stretching. After grafting with PHEMA, the additional peak at 1719 cm^{-1} was observed corresponding to C=O of acrylate. Also, there were the peaks at 1360 cm^{-1} and 1149 cm^{-1} which belong to -OH bending of primary alcohol (Radhakumary, Nair, Mathew, & Reghunadhan Nair, 2005).

Figure 3 presents the weight loss profiles (TG) and the derivative weight losses (DTG) of CS-*g*-PHEMA, CS, and PHEMA (homopolymer). Two weight losses were observed in CS, that is, the minor weight loss around 100 °C due to evaporation of absorbed water and the major weight loss at approximately 300 °C corresponding to deacetylation, de-polymerization, and thermal decomposition of CS (Georgieva, Zvezdova, & Vlaev, 2013). PHEMA also possessed two weight loss stages, that is, the first weight loss was at 100 °C and the second weight loss was around 400 °C belonging to thermal decomposition of PHEMA (Biryan, Demirelli, Torğut, & Pıhtılı, 2017). TG curve of CS-*g*-PHEMA shows two major weight losses at approximately at 250 °C and 500 °C attributed to the thermal decomposition of CS and grafted-PHEMA, respectively. DTG curves confirm two major weight losses of CS-*g*-PHEMA, in which the second peak temperature increased to 500 °C compared with that of PHEMA at 400 °C implying that PHEMA was chemically attached on CS. The residue of CS-*g*-PHEMA was less than that of CS indicating that the grafted-PHEMA was thermally decomposed to vaporized products while CS residue remains as non-volatile chars (Gawad, 2020).

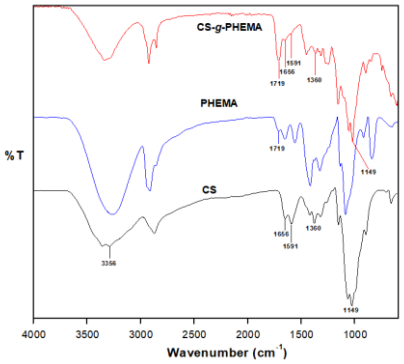

Figure 2. FT-IR spectra of CS, PHEMA, and CS-*g*-PHEMA

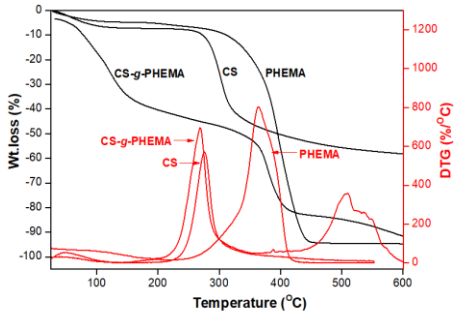

Figure 3. TG and DTG curves of CS, PHEMA, and CS-*g*-PHEMA

3.2 CS-g-PHEMA as corrosion inhibitor for mild steel

3.2.1 Inhibition efficiency (IE) and corrosion rate (R_{cor})

Figure 4a reveals the effect of CS and CS-*g*-PHEMA concentrations on the corrosion inhibition for mild steel. It is seen that IE increased proportionally to the concentration of either inhibitor, of which CS-*g*-PHEMA showed the better inhibition efficiency reaching IE as high as 91% at 500 ppm of CS-*g*-PHEMA. On the other hand, R_{cor} decreased almost linearly with CS or CS-*g*-PHEMA concentration, as presented in Figure 4b. The R_{cor} of CS-*g*-PHEMA were pronouncedly lower than that of CS for all concentrations. An improvement of IE and a lowering of R_{cor} arise from the effective adsorption of CS-*g*-PHEMA on the mild steel surface, enabled by the functional groups of heteroatoms, i.e., $-NH_2$ and -OH on CS and abundant -OH groups of the grafted-PHEMA (Dagdag *et al.*, 2019). Under acidic exposure to H_2SO_4, the SO_4^{2-} ions were adsorbed on mild steel surface rendering it negatively charged. At the same time, the polar $-NH_2$ and -OH groups of CS and CS-*g*-PHEMA are protonated, giving them positively charges. As a consequence, the adsorption of CS or CS-*g*-PHEMA takes place on the mild steel surface through electrostatic interactions. Additionally, N and O heteroatoms on CS and grafted-PHEMA can donate lone electrons to the vacant orbitals of Fe, thus inducing chemisorption of CS and CS-*g*-

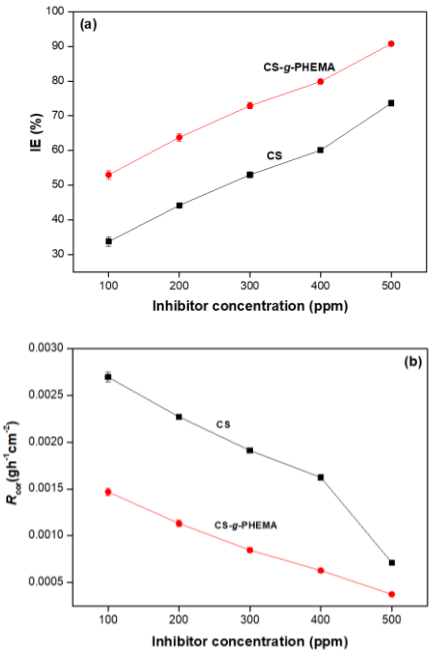

Figure 4. Effect of inhibitor treatment concentration on corrosion inhibition of mild steel: (a) inhibition efficiency, and (b) corrosion rate

PHEMA on the mild steel surface (Umoren, Banera, & Gervasi, 2013). Since the CS-*g*-PHEMA has more abundance of the heteroatoms -NH_2, -OH, and -C=O than does CS, the CS-*g*-PHEMA is preferentially adsorbed on mild steel surface with a larger adsorbed amount, resulting in better corrosion inhibition than that by CS.

The corrosion process can further be investigated thermodynamically according to the following equations (6) and (7) (Tourabi *et al*., 2014).

$$\ln R_{cor} = lnA - \frac{E_a}{RT} \quad (6)$$

$$\ln \frac{R_{cor}}{T} = \ln \frac{R}{Nh} + \frac{\Delta S^*}{R} - \frac{\Delta H^*}{RT} \quad (7)$$

where E_a is the activation energy of corrosion, A is the frequency factor, and ΔH^* and ΔS^* are the enthalpy and the entropy of activation for the corrosion. N and h are Avogadro's number and Planck's constant, respectively.

Table 1 summarizes the thermodynamic parameters. E_a increased from 19.4 kJ/mol for the mild steel blank to 46.7 kJ/mol and 72.7 kJ/mol upon adsorption of CS and CS-*g*-PHEMA, respectively. This indicates that the inhibitors hinder the corrosion by heightening the energy barrier for corrosion reactions. The increase of E_a above 40 kJ/mol after introducing CS and CS-*g*-PHEMA arises from blocking of active (dissolution) sites on the mild steel surface, resulting in a diffusion-controlled corrosion reaction (Fouda, El-Dossoki, & Shady, 2018). The large E_a of CS and CS-*g*-PHEMA suggest that their adsorption on the mild steel involves chemisorption. Furthermore, CS-*g*-PHEMA possessed higher energy barrier than did CS, thus offering more effective corrosion inhibition. The positive value of ΔH^* for the blank indicates endothermic mild steel dissolution, while CS and CS-*g*-PHEMA increased ΔH^*, because the formation of activated-complex from the inhibitors is the rate determining step of mild steel dissolution and hindered steel corrosion (Umoren *et al*., 2013). In addition, the positive ΔH^* affirms the chemisorption of CS and CS-*g*-PHEMA (Durnie *et al*., 1999). ΔS^*, on the other hand, were negative and became less negative in the presence of CS and CS-*g*-PHEMA. A negative ΔS^* indicates an associative mechanism in steel dissolution, and upon adsorption of CS or CS-*g*-PHEMA, the dissolution of mild steel became less favorable (Umoren & Solomon, 2014).

3.2.2 Potentiodynamic polarization

The potentiodynamic polarization curves (Tafel plots) of the mild steel in 0.2 M H_2SO_4 solution with CS and CS-*g*-PHEMA are presented in Figure 5. Accordingly, the important parameters corrosion current density (i_{corr}), anodic Tafel slope (β_a) and cathodic Tafel slope (β_c) derived from the extrapolation of anodic and cathodic linear regions to corrosion potential (E_{corr}) in the Tafel plots are summarized in Table 1. Compared with the blank, the presence of CS and CS-g-PHEMA remarkably decreased i_{corr}, more so with CS-*g*-PHEMA than with CS. Moreover, increasing the inhibitor concentrations decreased i_{corr} so that CS-*g*-PHEMA at 500 ppm exhibited the maximum inhibition efficiency reaching 90.7% IE.

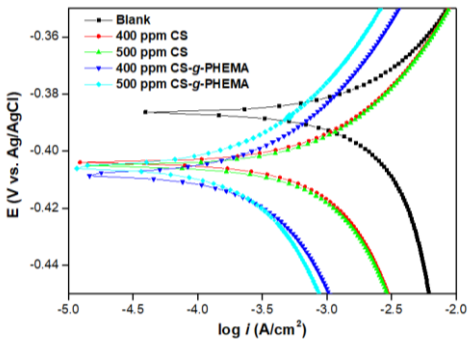

Figure 5. Potentiodynamic polarization curves (Tafel plots) of mild steel in 0.2 M H_2SO_4 after pretreatments with CS or CS-*g*-PHEMA at various concentrations

Table 1. Corrosion parameters from Tafel plots of mild steel in 0.2 M H_2SO_4 solution after pretreatments with various concentrations of inhibitors

	Blank	CS		CS-*g*-PHEMA	
		400 ppm	500 ppm	400 ppm	500 ppm
Current density, i_{corr} (μA/cm²)	1584.9	489.8	426.6	166.0	147.9
Anodic Tafel slope, β_a (mV/dec)	28.32	31.75	27.50	29.84	33.71
Cathodic Tafel slope, β_c (mV/dec)	39.61	42.33	39.11	42.89	43.38
Corrosion potential, E_{corr} (mV)	-386.4	-403.5	-404.6	-408.3	-405.8
Inhibition efficiency, IE_P (%)	-	69.10	73.08	89.53	90.67

The anodic and cathodic Tafel slopes were obtained from the decrease of i_{corr} in the linear regions. For CS-*g*-PHEMA, both β_a and β_c were higher than those of blank and they increased with CS-*g*-PHEMA concentration. The increase of both Tafel slopes confirms that CS-*g*-PHEMA was retarding the anodic oxidation and the cathodic reduction of mild steel surface. This is due to the adsorbed CS-*g*-PHEMA limiting the diffusion of H_3O^+ ions from bulk solution to undergo anodic metal dissolution and cathodic hydrogen evolution, as demonstrated schematically in Figure 6. In the case of CS, although both β_a and β_c were relatively high at 400 ppm, as CS concentration increased to 500 ppm they decreased and became close to those of the blank. This is possibly due to the strong attraction, via H-bonding, between CS molecules under high concentration leading to desorption of CS from the steel surface. On the other hand, the grafted-PHEMA with abundant -OH and -C=O functional groups offers a better adsorption on the mild steel surface. The E_{corr} with and without the inhibitors was less than 85 mV, indicating that CS-*g*-PHEMA and CS behave as mixed-type inhibitors, for which the corrosion inhibition is attributable to physical or chemical adsorption of the inhibitor molecules (Tang, 2019).

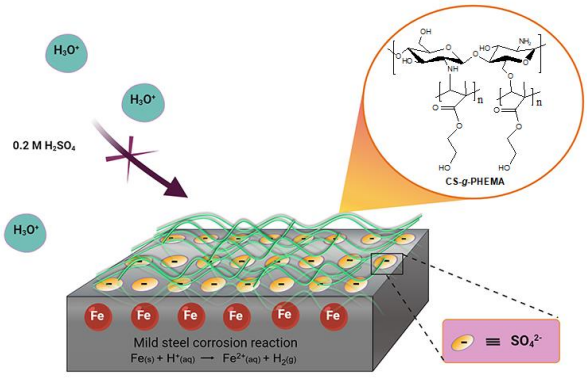

Figure 6. Schematic illustration of corrosion inhibition by CS-*g*-PHEMA

4. Conclusions

Biopolymer-based corrosion inhibitor from CS was successfully synthesized by using an ultrasound-assisted method for grafting with PHEMA. The ultrasound induced cavitation in CS aqueous solution, which induced sonolysis of the TBHP initiator producing active radicals. These radicals abstracted protons from CS generating active grafting sites, so that after introducing the HEMA monomer the graft polymerization could proceed at the grafting sites on CS, yielding CS-*g*-PHEMA. The synthesized CS-*g*-PHEMA was employed as a candidate corrosion inhibitor on mild steel, tested under acidic exposure to 0.2 M H_2SO_4. The corrosion test by gravimetry suggests that CS-*g*-PHEMA adsorbed preferentially on the mild steel surface compared to plain CS. As a consequence, the IE of CS-*g*-PHEMA was higher reaching 90% for the 500 ppm pretreatment, while the R_{cor} with CS-*g*-PHEMA was twice lower than that with CS pretreatment. Furthermore, the activation energies E_a of corrosion were estimated to be 46.7 kJ/mol and 72.7 kJ/mol with CS and CS-*g*-PHEMA treatments, respectively, indicating a higher energy barrier for the corrosion reactions with CS-*g*-PHEMA treatment. Potentiodynamic polarization runs were performed to investigate the corrosion reactions on mild steel, and they clearly showed the superior effect of CS-*g*-PHEMA in retarding anodic oxidation and cathodic reduction of the mild steel surface. This is because the adsorbed CS-*g*-PHEMA limits the diffusion of H_3O^+ to undergo anodic metal dissolution and cathodic hydrogen evolution on the mild steel surface.

Acknowledgements

This project is supported by Research and Graduate Studies, Khon Kaen University (Grant no. RP64-8-001). The partial support from Center of Excellence for Innovation in Chemistry (PERCH-CIC), Ministry of Higher Education, Science, Research and Innovation, Thailand is also acknowledged. The financial supports for S. N. Dalhatu doctoral research program from Tetfund Nigeria and Kano University of Science and Technology Wudil are highly appreciated. S. Khoonsap would like to thank Materials Chemistry Research Center (MCRC-KKU), Khon Kaen University, for the post-doctoral research assistantship.

References

Abdallah, M., Fawzy, A., & Hawsawi, H. (2020). Maltodextrin and chitosan polymers as inhibitors for the corrosion of carbon steel in 1.0 M hydrochloric acid. *International Journal of Electrochemical Science*, *15*, 5650–5663. doi:10.20964/2020.06.82

Alguaci, F. J. (2020). Adsorption processing for the removal of toxic Hg (II) from liquid effluents : Advances in the 2019 year. *Metals*, *10*(3), 412. doi:10.3390/met10030412

Aljeaban, N. A., Goni, L. K. M. O., Alharbi, B. G., Jafar, M. A., Ali, S. A., Chen, T., . . . Al-Muallem, H. A. (2020). Polymers decorated with functional motifs for mitigation of steel corrosion: An overview. *International Journal of Polymer Science*, *2020*, 1-23. doi:10.1155/2020/9512680

Argüelles-Monal, W. M., Lizardi-Mendoza, J., Fernández-Quiroz, D., Recillas-Mota, M. T., & Montiel-Herrera, M. (2018). Chitosan derivatives: Introducing new functionalities with a controlled molecular architecture for innovative materials. *Polymers*, *10*(3). doi:10.3390/POLYM10030342

Biryan, F., Demirelli, K., Torğut, G., & Pıhtılı, G. (2017). Synthesis, thermal degradation and dielectric properties of poly**[**2-hydroxy,3-(1-naphthyloxy) propylmethacrylate**]**. *Polymer Bulletin*, *74*(2), 583–602. doi:10.1007/s00289-016-1731-2

Chang, S. J., Niu, C. C., Huang, C. F., & Kuo, S. M. (2007). Evaluation of chitosan-g-PEG copolymer for cell anti-adhesion application. *Journal of Medical and Biological Engineering*, *27*(1), 41–46.

Dagdag, O., El Harfi, A., El Gouri, M., Safi, Z., Jalgham, R. T. T., Wazzan, N., . . . Pramod Kumar, U. (2019). Anticorrosive properties of Hexa (3-methoxy propan-1,2-diol) cyclotri-phosphazene compound for carbon steel in 3% NaCl medium: Gravimetric, electrochemical, DFT and Monte Carlo simulation studies. *Heliyon*, *5*(3). doi:10.1016/j.heliyon.2019.e01340

Devi, L., Sharma, R., & Singh, A. (2016). Synthesis and characterization of chitosan based graft copolymers with binary vinyl monomers for controlled drug release application. *Drug Delivery Letters*, *5*(3), 215–227. doi:10.2174/2210303106666160220005331

Deyab, M. A., Essehli, R., & El Bali, B. (2015). ChemInform abstract: Inhibition of copper corrosion in cooling seawater under flowing conditions by novel pyrophosphate. *ChemInform*, *46*(41). doi:10.1002/chin.201541014

Fouda, A. S., El-Dossoki, F. I., & Shady, I. A. (2018). Adsorption and corrosion inhibition behavior of polyethylene glycol on α-brass alloy in nitric acid solution. *Green Chemistry Letters and Reviews*, *11*(2), 67–77. doi:10.1080/17518253.2018.1438525

Gawad, O. F. A. (2020). Graft modification of carboxymethyl chitosan with styrene and its biological applications. *Beni-Suef University Journal of Basic and Applied Sciences 9*, *4*(2020). Retrieved from https://bjbas.springeropen.com/articles/10.1186/s43088-019-0019-7

Georgieva, V., Zvezdova, D., & Vlaev, L. (2013). Non-isothermal kinetics of thermal degradation of chitin. *Journal of Thermal Analysis and Calorimetry*, *111*(1), 763–771. doi:10.1007/s10973-012-2359-6

Kausalya, T., & Hazlina, H. (2020). Review on corrosion inhibitors for oil and gas corrosion issues. *Applied Sciences*, *10*(10), 3389. doi:10.3390/app10103389

Kimura, T., Sakamoto, T., Leveque, J. M., Sohmiya, H., Fujita, M., Ikeda, S., & Ando, T. (1996). Standardization of ultrasonic power for sono chemical reaction. *Ultrasonics Sonochemistry*, *3*(3), S157-S161. doi:10.1016/S1350-4177(96)00021-1

Li, B., Elango, J., & Wu, W. (2020). Recent advancement of molecular structure and biomaterial function of chitosan from marine organisms for pharmaceutical and nutraceutical application. *Applied Sciences* (*Switzerland*), *10*(14), 30–50. doi:10.3390/app10144719

Mason, T. J., & Lorimer, J. P. (2002). *Applied sonochemistry*: *The uses of power ultrasound in chemistry and processing*. Ann Arbor, MI: Wiley.

McKenzie, T. G., Karimi, F., Ashokkumar, M., & Qiao, G. G. (2019). Ultrasound and sonochemistry for radical polymerization: Sound synthesis. *Chemistry - A European Journal*, *25*(21), 5372–5388. doi:10.1002/chem.201803771

Rabizadeh, T., & Khameneh Asl, S. (2019). Chitosan as a green inhibitor for mild steel corrosion: Thermodynamic and electrochemical evaluations. *Materials and Corrosion*, *70*(4), 738–748. doi:10.1002/maco.201810501

Radhakumary, C., Nair, P. D., Mathew, S., & Reghunadhan Nair, C. P. (2005). Biopolymer composite of chitosan and methyl methacrylate for medical applications. *Trends in Biomaterials and Artificial Organs*, *18*(2), 117–124.

Sanaeishoar, H., Sabbaghan, M., & Argyropoulos, D. S. (2018). Ultrasound assisted polyacrylamide grafting on nano-fibrillated cellulose. *Carbohydrate Polymers*, *181*(September), 1071–1077. doi:10.1016/j.carbpol.2017.11.042

Tang, Z. (2019). A review of corrosion inhibitors for rust preventative fluids. *Current Opinion in Solid State and Materials Science*, *23*(4), 1–16. doi:10.1016/j.cossms.2019.06.003

Tourabi, M., Nohair, K., Nyassi, A., Hammouti, B., Jama, C., & Bentiss, F. (2014). Thermodynamic characteri zation of metal dissolution and inhibitor adsorption processes in mild steel/3,5-bis(3,4-dimethoxy phenyl)-4-amino-1,2,4-triazole/hydrochloric acid system. *Journal of Materials and Environmental Science*, *5*(4), 1133–1143.

Umoren, S., Banera, M. J., & Gervasi, C. (2013). Inhibition of mild steel corrosion in HCl solution using chitosan Inhibition of mild steel corrosion in HCl solution using chitosan. *Cellulose*, *20*, 2529–2545. doi:10.1007/s10570-013-0021-5

Umoren, S. A., & Solomon, M. M. (2014). Recent developments on the use of polymers as corrosion inhibitors-a review. *Open Materials Science Journal*, *8*(1), 39–54. doi:10.2174/1874088X01408010039

Xu, S., Zhang, S., Guo, L., Feng, L., & Tan, B. (2019). Experimental and theoretical studies on the corrosion inhibition of carbon steel by two indazole derivatives in HCl medium. *Materials*, *12*(8), 1–11. doi:10.3390/ma12081339

Yadav, M., Sharma, U., & Yadav, P. N. (2013). Isatin compounds as corrosion inhibitors for N80 steel in 15% HCl. *Egyptian Journal of Petroleum*, *22*(3), 335–344. doi:10.1016/j.ejpe.2013.10.001